Cell Stem Cell

Brief Report

Cell Surface Mechanics Gate Embryonic Stem Cell Differentiation

Graphical Abstract

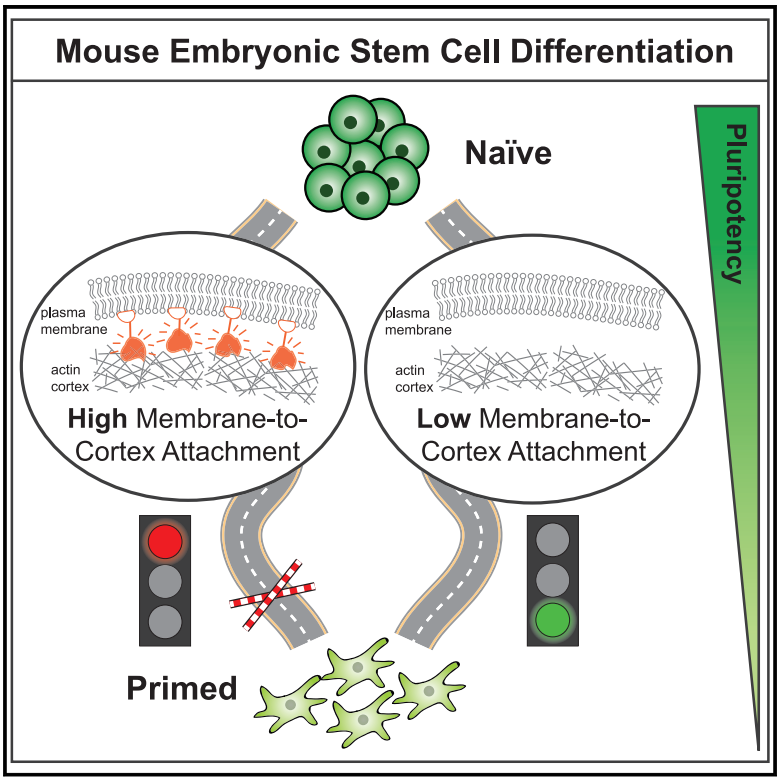

Highlights

- Early mESC differentiation is accompanied by a decrease in apparent membrane tension
- Differentiating mESCs decrease their membrane-to-cortex attachment (MCA)
- Development of a signaling-inert MCA (iMC) linker
- MCA reduction is necessary but not sufficient for naive-to-primed transition

Authors

Martin Bergert, Sergio Lembo, Sumana Sharma, ..., Jamie A. Hackett, Evangelia Petsalaki, Alba Diz-Muñoz

Correspondence

diz@embl.de

In Brief

Bergert et al. use biophysical methods to investigate the role of cell surface mechanics during stem cell differentiation. They show that naive cells release their plasma membrane from the underlying actin cortex when transitioning to a primed state. Preventing this detachment forces cells to retain a naive pluripotent identity.

Bergert et al., 2021, Cell Stem Cell *28*, 209–216
February 4, 2021
https://doi.org/10.1016/j.stem.2020.10.017

CellPress

Cell Stem Cell

CellPress
OPEN ACCESS

Brief Report

Cell Surface Mechanics Gate Embryonic Stem Cell Differentiation

Martin Bergert,[1,6] Sergio Lembo,[1,5,6] Sumana Sharma,[2] Luigi Russo,[1,5] Danica Milovanović,[1] Kristjan H. Gretarsson,[3] Mandy Börmel,[4] Pierre A. Neveu,[1] Jamie A. Hackett,[3] Evangelia Petsalaki,[2] and Alba Diz-Muñoz[1,7,*]

[1]Cell Biology and Biophysics Unit, European Molecular Biology Laboratory, Meyerhofstrasse 1, 69117 Heidelberg, Germany
[2]European Bioinformatics Institute, European Molecular Biology Laboratory, Hinxton CB10 1SD, UK
[3]Epigenetics and Neurobiology Unit, European Molecular Biology Laboratory, Via Ramarini 32, 00015 Monterotondo, Italy
[4]Electron Microscopy Core Facility, European Molecular Biology Laboratory, Meyerhofstrasse 1, 69117 Heidelberg, Germany
[5]Collaboration for joint PhD degree between EMBL and Heidelberg University, Faculty of Biosciences.
[6]These authors contributed equally
[7]Lead Contact
*Correspondence: diz@embl.de
https://doi.org/10.1016/j.stem.2020.10.017

SUMMARY

Cell differentiation typically occurs with concomitant shape transitions to enable specialized functions. To adopt a different shape, cells need to change the mechanical properties of their surface. However, whether cell surface mechanics control the process of differentiation has been relatively unexplored. Here we show that membrane mechanics gate exit from naive pluripotency of mouse embryonic stem cells. By measuring membrane tension during early differentiation, we find that naive stem cells release their plasma membrane from the underlying actin cortex when transitioning to a primed state. By mechanically tethering the plasma membrane to the cortex by enhancing Ezrin activity or expressing a synthetic signaling-inert linker, we demonstrate that preventing this detachment forces stem cells to retain their naive pluripotent identity. We thus identify a decrease in membrane-to-cortex attachment as a new cell-intrinsic mechanism that is essential for stem cells to exit pluripotency.

INTRODUCTION

During development of most multicellular organisms, spherical totipotent cells give rise to differentiated cells with all of the dramatically different morphologies present in the adult body. Acquisition of fate and changes in cell shape often emerge concurrently. Cell shape is determined by surface mechanics and interactions with the extracellular environment. Although cell-matrix interactions have been shown to be necessary (Chowdhury et al., 2010a; Murray et al., 2013) and, in some cases, sufficient (Engler et al., 2006) for differentiation, it remains unknown whether and how cell-intrinsic surface mechanics regulate fate. A particularly striking example of identity and shape change is the transition from the naive to the primed pluripotent state during early differentiation of mouse embryonic stem cells (mESCs). Naive cells grow in compact colonies (Figures 1A–1C) and maintain this state when cultured in the presence of 2i/LIF. 2i/LIF removal releases the differentiation blockade, and naive colonies flatten rapidly (within 24–48 h) into a monolayer of primed cells that grow lamellipodium-like protrusions in a process reminiscent of epithelial-to-mesenchymal transition (Mulas et al., 2019; Figures 1A–1C; Video S1). Such cell spreading is necessary to drive exit from naive pluripotency because naive cells plated on soft substrates, where they cannot spread, do not transition to a primed state (Chowdhury et al., 2010a).

Cell spreading (Gauthier et al., 2011) and migration, and specifically the size of the leading edge as well as the rate of lamellipodium extension (Houk et al., 2012; Raucher and Sheetz, 2000), are regulated by plasma membrane tension, defined as the energetic cost of increasing a membrane area. Given the striking morphological change and the large protrusions primed stem cells display, we hypothesized that membrane tension may have an important regulatory role during exit from naive pluripotency.

RESULTS

To assess whether and how surface mechanics regulate cell state, we first measured apparent membrane tension by static tether pulling via single-cell atomic force spectroscopy, where a plasma membrane tether is held by an atomic force microscopy cantilever with a constant length until it breaks (Figure 1D). Comparing naive and primed cells, we found that the static tether force was reduced significantly in primed cells (from 41.3 ± 5.25 to 30 ± 5.92 pN; Figure 1F). Such a decrease in static tether force corresponds to an almost 50% reduction in apparent

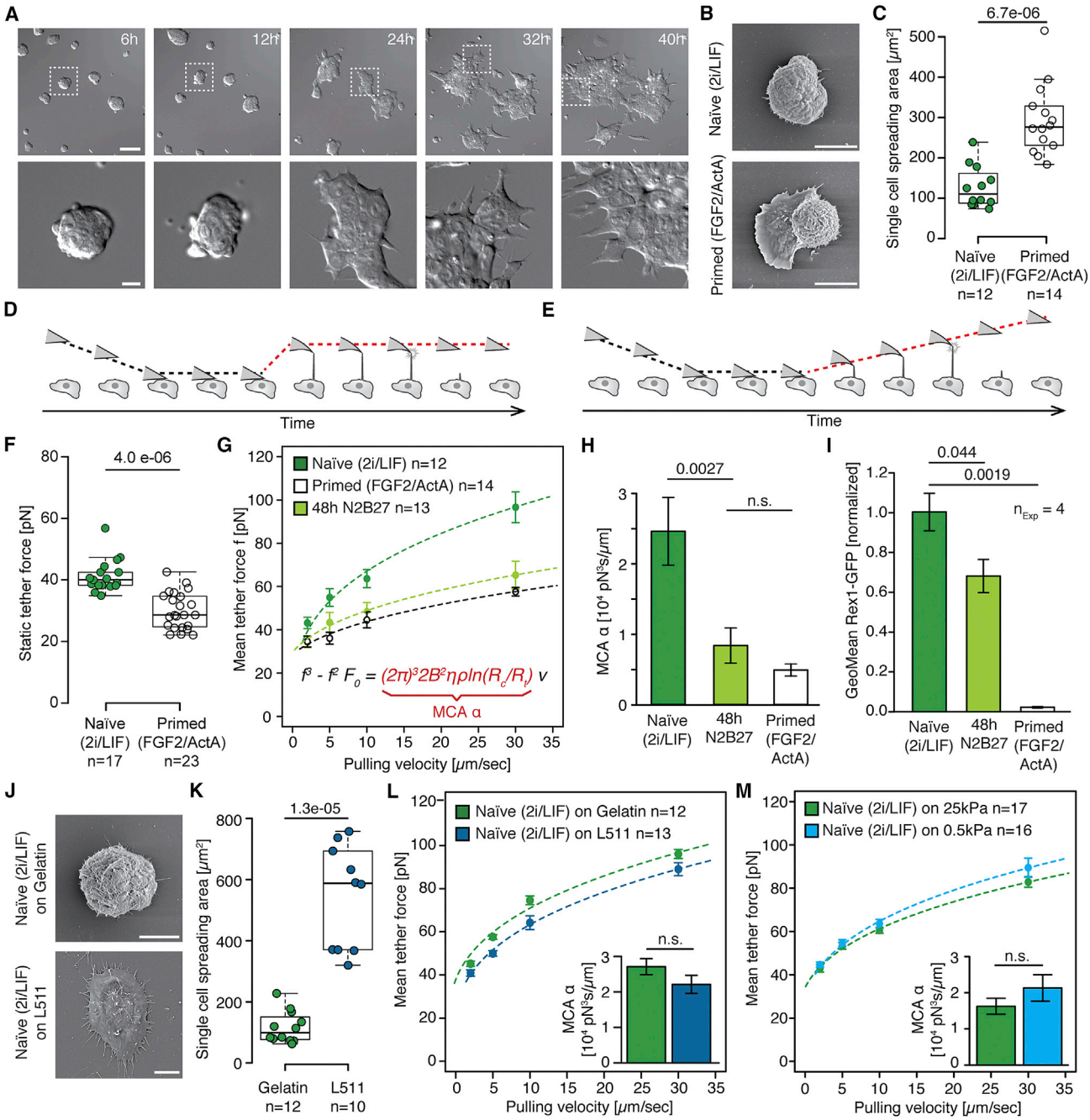

Figure 1. During Exit from Naive Pluripotency, Cells Spread with a Concomitant Reduction in Apparent Membrane Tension and MCA

(A) Representative bright-field (differential interference contrast [DIC]) images of Rex1-GFPd2 mESCs during exit from pluripotency in plain N2B27 medium. The bottom panel corresponds to a magnification of the boxed region in the top panel. See also Video S1. Scale bars, 50 μm (top panel), 10 μm (bottom panel).

(B) Representative scanning electron microscopy images of naive (2i/LIF) and primed (FGF2/ActA) Rex1-GFPd2 mESCs. Scale bar, 10 μm.

(C) Single-cell spreading area quantified from scanning electron microscopy images. n, number of cells analyzed; p value, Welch's t test.

(D) Schematic of static tether pulling using atomic force spectroscopy.

(E) Schematic of dynamic tether pulling using atomic force spectroscopy.

(F) Mean static tether force of naive (2i/LIF) and primed (FGF2/ActA) Rex1-GFPd2 mESCs. n, number of cells analyzed in 2 independent experiments; p value, Mann-Whitney *U* test.

(G) Force-velocity curve from dynamic tether pulling on Rex1-GFPd2 mESCs in 2i/LIF medium, during exit from pluripotency in N2B27 medium at 48 h, and primed in FGF2/ActA medium. Data points are mean tether force f ± SEM at 2, 5, 10, and 30 μm/s pulling velocity. n, number of cells analyzed in 3 independent experiments.

(H) Mean and standard deviation of the MCA parameter *a* obtained from Monte Carlo-based fitting (see STAR Methods for details); p value, *Z* test.

(legend continued on next page)

membrane tension (from 80 to 42 μN/m; see STAR Methods for details).

That primed cells have a lower membrane tension seems paradoxical given their shape (Figures 1B and 1C) because leading-edge growth and cell spreading are known to increase apparent membrane tension (Gauthier et al., 2011; Houk et al., 2012). Static tether pulling measures the combination of in-plane membrane tension (originating from the tight packing of hydrophobic lipid molecules to avoid contact with water molecules) as well as protein-mediated attachment to the underlying actomyosin cortex (termed membrane-to-cortex attachment [MCA]), which also constrains a membrane area increase (Brochard-Wyart et al., 2006; Hochmuth et al., 1996; reviewed in Diz-Muñoz et al., 2018). To determine which of these two mechanical parameters changes during stem cell differentiation, we specifically measured MCA by dynamic tether pulling (Figure 1E), which measures the force required to extrude plasma membrane tethers across a range of different velocities (Brochard-Wyart et al., 2006; Diz-Muñoz et al., 2010; see STAR Methods for details). We found that MCA is about 3-fold larger in naive mESCs compared with cells locked in the primed state by culture in medium containing FGF2/ActA (fibroblast growth factor 2 and Activin A; Brons et al., 2007; Wray et al., 2011; Figures 1G and 1H, naive versus primed). This reduction in MCA is also present during cell spreading following 2i/LIF removal, which allows exit from naive pluripotency into the primed state in 24–48 h (Mulas et al., 2019; Figures 1G and 1H, naive versus 48 h N2B27). Thus, irrespective of whether cells are locked in the primed state or exiting from naive pluripotency (as mirrored by the expression level of the naive maker Rex1-GFPd2; Toyooka et al., 2008; Wray et al., 2011; Figure 1I), MCA levels decreased significantly.

Because MCA reduction and cell spreading occur simultaneously (Figures 1A, 1C, 1G, and 1H), we next investigated the relationship between MCA, cell shape, and the extracellular environment; because the latter has been shown to affect cell shape (Trappmann et al., 2012) and identity (Chowdhury et al., 2010a). To this end, we first forced naive cells to spread by plating them on Laminin 511 (L511) in the presence of 2i/LIF (Figures 1J and 1K) and measured their MCA level. We found no significant difference between round cells on gelatin and spread cells on L511 (Figure 1L), showing (1) that an increase in cell area alone does not significantly affect MCA and (2) that MCA is independent of the chemical composition of the extracellular matrix. Moreover, we assessed the effect of substrate stiffness on MCA and found no substantial differences between cells plated on 0.5- or 25-kPa hydrogels (Figure 1M), mimicking a range of tissue stiffness from brain-like to cartilage-like (Guimarães et al., 2020). The pluripotency state of cells is not perturbed by these variations of the chemical or mechanical composition of the extracellular environment (Figures S1A–S1D). We therefore conclude that MCA is a cell-autonomous property and that, during exit from naive pluripotency, mESCs specifically decrease tethering of their plasma membrane to cortical actin.

Given their co-occurrence, we next investigated whether the reduction in MCA was upstream (i.e., a regulator) or downstream (i.e., a consequence) of exit from naive pluripotency. To this end, we first expressed constitutively active Ezrin (CAEzrin, T567D; Gautreau et al., 2000) tagged with mCherry in an inducible manner in naive mESCs (Figures 2A and S1E). Ezrin links the plasma membrane to the underlying cortex, and CAEzrin is the current gold standard to experimentally increase MCA (Liu et al., 2012; Stefani et al., 2017). We then monitored MCA levels during exit from naive pluripotency and found that CAEzrin expressing mESCs maintained a high MCA with values similar to naive mESCs, in stark contrast to the strongly decreased MCA of uninduced controls (Figure 2B). This shows that CAEzrin expression prevents the decrease in MCA seen during early mESC differentiation. In addition to linking the plasma membrane to the cell cortex, Ezrin also has critical biochemical roles in several signaling cascades (reviewed in Fehon et al., 2010). To rule out Ezrin's biochemical functions and to unambiguously test a purely mechanical role of MCA during exit from naive pluripotency, we engineered a synthetic molecular tool that directly links the plasma membrane to actin but is inert regarding signaling (iMC-linker; Figure 2C). It consists of a minimal actin binding domain (from Utrophin) fused to mCherry for fluorescence visualization and tagged with a lipidation consensus sequence (from Lyn) for plasma membrane insertion (see STAR Methods for details). The iMC-linker as well as its individual components localized to the cell surface when expressed in mESCs in an inducible manner (Figures 2D, S1F, and S1G). Inducing iMC-linker expression also forced stem cells to retain a high MCA even 48 h after allowing differentiation by 2i/LIF removal (Figure 2E), similarly to CAEzrin expression.

With two orthogonal constructs at hand that prevent the decrease of MCA during early mESC differentiation, we next investigated whether forcing cells to keep a high MCA state by expression of CAEzrin or the iMC-linker affects their ability to exit naive pluripotency. First, we assessed the expression levels of the pluripotency marker Nanog in control and CAEzrin or iMC-linker-expressing cells at 48 h by immunofluorescence. We found that cells with high MCA display elevated Nanog levels compared with uninduced controls (Figure 2F), suggesting that cells retain a more naive identity. To dynamically evaluate exit from naive pluripotency in living cells, we used Rex1-GFPd2 cells (Toyooka et al., 2008; Wray et al., 2011). Indeed, 48 h after

(I) Normalized GFP geometric mean intensities for Rex1-GFPd2 mESCs in 2i/LIF medium, during exit from pluripotency in N2B27 medium at 48 h, and primed in FGF2/ActA medium. n_{Exp}, number of independent experiments; error bars, SEM; p values, Welch's t test.

(J) Representative scanning electron microscopy images of naive (2i/LIF) Rex1-GFPd2 mESCs on gelatin or on Laminin 511 (L511). Scale bar, 10 μm.

(K) Single-cell spreading area quantified from scanning electron microscopy images. n, number of cells analyzed; p value, Welch's t test.

(L) Force-velocity curve from dynamic tether pulling on naive (2i/LIF) Rex1-GFPd2 mESCs plated on gelatin or on L511. Data points are mean f ± SEM at 2, 5, 10, and 30 μm/s pulling velocity. n, number of cells analyzed in 3 independent experiments. The inset shows mean and standard deviation of the MCA parameter *a* obtained from Monte Carlo-based fitting (see STAR Methods for details); p value, *Z* test.

(M) Force-velocity curve from dynamic tether pulling on Rex1-GFPd2 mESCs in 2i/LIF medium after plating for 48 h on L511-coated hydrogels of 25-kPa or 0.5-kPa stiffness. Data points are mean f ± SEM at 2, 5, 10, and 30 μm/s pulling velocity. n, number of cells analyzed in 4 independent experiments. The inset shows mean and standard deviation of the MCA parameter *a* obtained from Monte Carlo-based fitting (see STAR Methods for details); p value, *Z* test.

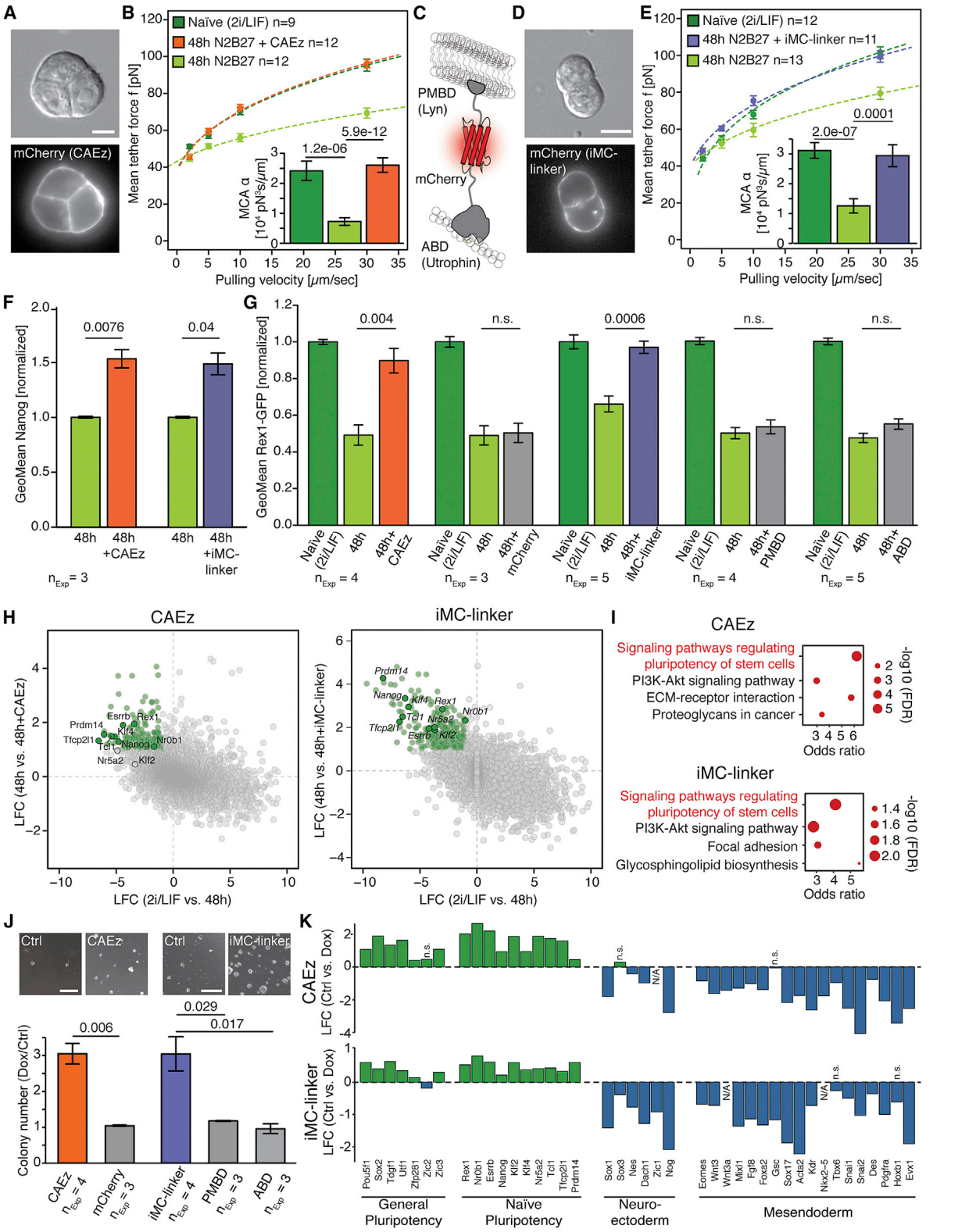

Figure 2. CAEzrin and the Synthetic iMC-Linker Gate Exit from Naive Pluripotency by Maintaining High MCA

(A) Representative bright-field (DIC) and fluorescent images of naive Rex1-GFPd2 *ind*-CAEz mESCs expressing CAEz-mCherry in 2i/LIF+Dox medium. Scale bar, 10 μm.

(legend continued on next page)

2i/LIF removal, CAEzrin- or iMC-linker-expressing cells retained high levels of Rex1, very similar to naive stem cells, in contrast to control cells expressing only mCherry or individual iMC-linker components (Figure 2G). The Nanog and Rex1-GFPd2 levels strongly suggest that a high MCA state forces stem cells to retain a naive pluripotent identity. To obtain a more global picture of the status of the cellular transcriptome with high MCA, we performed RNA sequencing (RNA-seq) during a time course upon 2i/LIF removal of induced and uninduced CAEzrin and iMC-linker cells. We consistently found that expression of a variety of key naive pluripotency genes (Kalkan et al., 2017) is elevated in cells with high MCA (Figures S1H and S1I). Moreover, we observed that the self-organizing network of transcription factors that governs naive pluripotency (Niwa, 2007) is upregulated in CAEzrin- and iMC-linker-expressing cells (top KEGG [Kyoto Encyclopedia of Genes and Genomes] database enriched pathway: ''signalling pathways regulating pluripotency of stem cells''; Figures 2H and 2I). We orthogonally tested the effect of CAEzrin and iMC-linker expression on naive pluripotency by assessing global DNA methylation (DNAme). DNAme is a key marker of exit from pluripotency, and cells typically undergo a transition from DNA hypomethylation (20%–40%) to hypermethylation (60%–80%) upon 2i/LIF withdrawal (Hackett et al., 2013; 2018; Leitch et al., 2013). We found that induction of CAEzrin or iMC-linker expression significantly impaired acquisition of global DNA hypermethylation (Figure S1J). We conclude that cells that maintain high MCA upon 2i/LIF removal because of the presence of ectopic membrane-to-cortex linkers exhibit general naive pluripotency features within their transcriptional as well as epigenetic landscapes. Finally, to functionally test those naive features, we challenged CAEzrin- and iMC-linker-expressing cells in a re-plating assay, which assesses dissolution of the core pluripotency gene regulatory network by testing the ability of differentiating cells to survive under stringent 2i/LIF medium conditions (Betschinger et al., 2013; Cirera-Salinas and Ciaudo, 2017; Figure S1K; see STAR Methods for details). Notably, CAEzrin and iMC-linker cells were able to generate 3-fold more colonies than their control counterparts expressing only mCherry or individual iMC-linker components (Figure 2J). This shows that CAEzrin and iMC-linker expression forces cells to retain a naive pluripotent identity even in the absence of differentiation inhibitors. Our findings suggest a model in which maintaining high MCA significantly inhibits the ability of mESCs to exit naive pluripotency.

We then wanted to find out whether decreasing MCA is sufficient to drive naive-to-primed transition by expressing a dominant-negative version of Ezrin (DNEzrin, T567A; Gautreau et al., 2000; Figure S2A). As shown previously (Diz-Muñoz et al., 2010), DNEzrin led to a decrease in MCA (Figure S2B), but its expression failed to downregulate pluripotency markers (Figures S2C and S2D). Additionally, upon 2i/LIF removal, the Rex1 levels of DNEzrin-expressing cells were not decreased significantly compared with control cells (Figure S2E) and nor was the colony number in the re-plating assay (Figure S2F). These findings show that DNEzrin expression does not speed up naive-to-primed transition and suggest that MCA acts as a gate, not a driver, of exit from naive pluripotency.

Finally, we sought to investigate whether our findings are also relevant in other developmental differentiation contexts beyond the naive-to-primed transition of mESCs in 2D culture. To that end, we tested the effect of expressing CAEzrin or the iMC-linker during embryoid body formation, organoids where cells spontaneously differentiate into lineages of the three primary germ layers (Figure S1L). Specifically, we induced expression of our constructs for the first 48 h of embryoid body formation and assessed expression of general and naive pluripotency markers (Kalkan et al., 2017) as well as differentiation markers by RNA-seq after 2 additional days. Even in this more complex

(B) Force-velocity curve from dynamic tether pulling on Rex1-GFPd2 *ind*-CAEz mESCs in 2i/LIF medium and during exit from pluripotency in N2B27 ± Dox medium at 48 h. Data points are mean f ± SEM at 2, 5, 10, and 30 μm/s pulling velocity. n, number of cells analyzed in 3 independent experiments. The inset shows mean and standard deviation of the MCA parameter *a* obtained from Monte Carlo-based fitting (see STAR Methods for details); p value, *Z* test.

(C) Schematic of the iMC-linker. PMBD, plasma membrane-binding domain; ABD, actin-binding domain.

(D) Representative bright-field (DIC) and fluorescent images of naive Rex1-GFPd2 *ind*-iMC mESCs expressing the iMC-linker in 2i/LIF+Dox medium. Scale bar, 10 μm.

(E) Force-velocity curve from dynamic tether pulling on Rex1-GFPd2 *ind*-iMC mESCs in 2i/LIF medium and during exit from pluripotency in N2B27 ± Dox medium at 48 h. Data points are mean f ± SEM at 2, 5, 10, and 30 μm/s pulling velocity. n, number of cells analyzed in 3 independent experiments. The inset shows mean and standard deviation of the MCA parameter *a* obtained from Monte Carlo-based fitting (see STAR Methods for details); p value, *Z* test.

(F) Normalized geometric mean intensities of Nanog immunofluorescence levels for Rex1-GFPd2 *ind*-CAEz and *ind*-iMC mESCs plated for 48 h in N2B27 medium or N2B27+Dox medium. Error bars, SEM; p values, Welch's t test.

(G) Normalized GFP geometric mean intensities for Rex1-GFPd2 *ind*-CAEz, *ind*-mCherry, *ind*-iMC, *ind*-PMBD, and *ind*-ABD mESCs in 2i/LIF medium and during exit from pluripotency in N2B27 ± Dox medium at 48 h. Error bars, SEM; p value, Welch's t test.

(H) Comparison of mRNA fold-changes for Rex1-GFPd2 *ind*-CAEz and *ind*-iMC mESCs grown in 2i/LIF and N2B27+Dox media (48 h) with plain N2B27 medium (48 h). Naive pluripotency genes (Kalkan et al., 2017) were upregulated in cells grown in 2i/LIF medium and N2B27+Dox medium (top left quadrant; green: significantly enriched genes, log-fold change [LFC] > 1 and false discovery rate [FDR] < 0.05). Data are from 3 independent RNA-seq experiments.

(I) RNA-seq-derived enriched pathway maps for Rex1-GFPd2 *ind*-CAEz and *ind*-iMC mESCs in N2B27+Dox medium compared with plain N2B27 medium at 48 h. Significantly enriched genes (LFC > 1 and FDR < 0.05) from differential RNA-seq expression analysis were used to identify the enriched pathway maps from the KEGG database (see STAR Methods for details). Shown are the 4 most enriched pathway maps.

(J) Top: representative images of the re-plating assay for Rex1-GFPd2 *ind*-CAEz and *ind*-iMC mESCs. Scale bar, 500 μm. Bottom: normalized colony number (Dox/Ctrl) for Rex1-GFPd2 *ind*-CAEz, *ind*-mCherry, *ind*-iMC, *ind*-PMBD, and *ind*-ABD mESCs re-plated after 48-h exit in N2B27 ± Dox medium. Error bars, SEM; p value, Welch's t test.

(K) RNA-seq-derived mRNA fold changes of general and naive pluripotency markers (Kalkan et al., 2017) and markers for neuroectoderm and mesendoderm formation on day 4 of embryoid body differentiation for Rex-GFPd2 *ind*-CAEz (top) or *ind*-iMC (bottom) mESCs (data from 4 independent experiments). Green indicates higher and blue indicates lower expression in Dox-induced cells dissociated from embryoid bodies. N/A, expression below detection limits. All LFCs are significant (p < 0.01) except when noted otherwise (n.s.).

multicellular context, we observed that expression of CAEzrin or the iMC-linker is sufficient to maintain expression of the naive transcription network and delays upregulation of lineage-specific markers (Figure 2K). These results highlight that our model applies to a broader range of developmental contexts because high MCA favors retention of naive pluripotency even during germ layer formation in embryoid bodies.

DISCUSSION

Changing cell surface mechanics by modifying linkage of the plasma membrane to the underlying actomyosin cortex is likely to be important for embryonic stem cells *in vivo*. Ezrin, one of the most characterized MCA proteins, marks the outside-facing apical domains of 8- to 16-cell mouse embryos (Louvet et al., 1996). This apical domain is necessary and sufficient for the first lineage segregation in early mouse embryos (Korotkevich et al., 2017). Beyond the mouse, mechanical properties such as substrate stiffness, cortical contractility, fluid flow, cyclic stress, compression, and luminal pressure have been linked to differentiation in several species (Aguilar et al., 2016; Chan et al., 2019; Chowdhury et al., 2010b; Cohen and Chen, 2008; Engler et al., 2006; Farge, 2003; Hove et al., 2003; Li et al., 2018; Maître et al., 2016; North et al., 2009; Pathak et al., 2014; Przybyla et al., 2016). Using mechanics to control differentiation and development could provide robustness because physical forces and material properties often do not depend on the activity of a single gene. It will be interesting to explore in the future whether MCA has a regulatory role in other differentiation responses.

How exactly might lowering MCA gate exit from naive pluripotency? Previous studies have shown that membrane tension regulates several cellular functions, such as endocytosis (Gauthier et al., 2009; Rauch et al., 2002), phagocytosis (Masters et al., 2013), cell polarity (Houk et al., 2012), and formation of blebs or lamellipodia (Diz-Muñoz et al., 2010; 2016). In fact, a complementary parallel study suggests that endocytic control of FGF/ERK signaling acts downstream of membrane mechanics during the naive-to-primed transition (De Belly et al., 2020 [this issue of *Cell Stem Cell*]). However, such studies have used mechanical perturbations that also influence biochemical signaling and measured apparent membrane tension, which confounds several mechanical parameters. Thus, the specific functions of cell surface signal transduction versus mechanics as well as the relative contribution of the two membrane mechanics parameters, in-plane tension and MCA, have been impossible to disentangle. Our work, together with recent reports of a role in lamellipodium initiation (Bisaria et al., 2020; Welf et al., 2019), highlights MCA as a critical parameter for central cellular function. The synthetic iMC-linker developed here specifically manipulates MCA; thus, it will help us to understand how cell surface mechanics (and in particular MCA) control cell signaling and shape in a variety of processes, such as differentiation, polarity, and migration.

Limitations of Study

Because of the time required for a protein to be expressed under a doxycycline-inducible promoter, our time resolution is limited, and we cannot determine at which time point between 0–48 h MCA acts. Moreover, although we reproduced some of our findings in several clonal lines, others, like the RNA-seq or DNAme analysis, were only performed in one representative clonal line. In addition, it remains unclear what factors downstream of MCA contribute to sustaining the naive state. Furthermore, although we have shown that our findings are not only key for naive-to-primed transition but also affect other developmental processes, such as germ layer formation, we have not yet determined whether MCA forces cells to retain a naive identity in mouse or human blastocysts. Finally, we cannot comment on the penetrance of our phenotype because most of our assays are population based. Future studies using single-cell methods will be needed to assess whether some cells are blocked in a naive state or whether all cells display a delay in the naive-to-primed transition.

STAR★METHODS

Detailed methods are provided in the online version of this paper and include the following:

- KEY RESOURCES TABLE
- RESOURCE AVAILABILITY
  - Lead contact
  - Materials availability
  - Data and code availability
- EXPERIMENTAL MODEL AND SUBJECT DETAILS
  - Cell culture
  - Stable cell line generation
- METHOD DETAILS
  - Re-plating assay
  - Flow cytometry
  - Tether extrusion by atomic force spectroscopy
  - Tether data analysis and model assumptions
  - Scanning electron microscopy
  - RNA-sequencing
  - Nanog immunofluorescence
  - DNA methylation analysis
- QUANTIFICATION AND STATISTICAL ANALYSIS

SUPPLEMENTAL INFORMATION

Supplemental Information can be found online at https://doi.org/10.1016/j.stem.2020.10.017.

ACKNOWLEDGMENTS

We thank J. Ellenberg, T. Hiiragi, C.J. Chan, and E. Welf for critical reading of the manuscript. We thank A. Gopalan for help with substrates of controlled stiffness. We thank the EMBL flow cytometry core facility and the EMBL electron microscopy core facility for critical assistance and advice. We are also truly thankful to the EMBL genomics core facility (and in particular L. Villacorta and V. Benes) for speed record sequencing and critical support. This study was funded by the European Molecular Biology Laboratory (EMBL) (to A.D.M., P.A.N., E.P., and J.A.H.) and the Human Frontiers Science Program (HFSP) grant RGY0073/2018 (to A.D.M.). D.M. is the recipient of an Otto Bayer fellowship from the Bayer Foundation.

AUTHOR CONTRIBUTIONS

A.D.M., M. Bergert, and S.L. conceived the project and designed the experiments with stem cell advice from P.A.N. and J.A.H.. M. Bergert, S.L., D.M., L.R., K.H.G., and M. Börmel performed the experiments and analyzed the data. S.S. and E.P. analyzed the RNA-seq data. A.D.M. and M. Bergert wrote

the manuscript with input from S.L., J.A.H., P.N., S.S., and E.P. All authors contributed to the interpretation of the data and read and approved the final manuscript.

DECLARATION OF INTERESTS

The authors declare no competing interests.

Received: December 3, 2019
Revised: July 24, 2020
Accepted: October 28, 2020
Published: November 17, 2020

REFERENCES

Aguilar, A., Pertuy, F., Eckly, A., Strassel, C., Collin, D., Gachet, C., Lanza, F., and Léon, C. (2016). Importance of environmental stiffness for megakaryocyte differentiation and proplatelet formation. Blood *128*, 2022–2032.

Betschinger, J., Nichols, J., Dietmann, S., Corrin, P.D., Paddison, P.J., and Smith, A. (2013). Exit from pluripotency is gated by intracellular redistribution of the bHLH transcription factor Tfe3. Cell *153*, 335–347.

Bisaria, A., Hayer, A., Garbett, D., Cohen, D., and Meyer, T. (2020). Membrane-proximal F-actin restricts local membrane protrusions and directs cell migration. Science *368*, 1205–1210.

Brochard-Wyart, F., Borghi, N., Cuvelier, D., and Nassoy, P. (2006). Hydrodynamic narrowing of tubes extruded from cells. Proc. Natl. Acad. Sci. USA *103*, 7660–7663.

Brons, I.G.M., Smithers, L.E., Trotter, M.W.B., Rugg-Gunn, P., Sun, B., Chuva de Sousa Lopes, S.M., Howlett, S.K., Clarkson, A., Ahrlund-Richter, L., Pedersen, R.A., and Vallier, L. (2007). Derivation of pluripotent epiblast stem cells from mammalian embryos. Nature *448*, 191–195.

Chan, C.J., Costanzo, M., Ruiz-Herrero, T., Mönke, G., Petrie, R.J., Bergert, M., Diz-Muñoz, A., Mahadevan, L., and Hiiragi, T. (2019). Hydraulic control of mammalian embryo size and cell fate. Nature *571*, 112–116.

Chowdhury, F., Li, Y., Poh, Y.-C., Yokohama-Tamaki, T., Wang, N., and Tanaka, T.S. (2010a). Soft substrates promote homogeneous self-renewal of embryonic stem cells via downregulating cell-matrix tractions. PLoS ONE *5*, e15655.

Chowdhury, F., Na, S., Li, D., Poh, Y.-C., Tanaka, T.S., Wang, F., and Wang, N. (2010b). Material properties of the cell dictate stress-induced spreading and differentiation in embryonic stem cells. Nat. Mater. *9*, 82–88.

Cirera-Salinas, D., and Ciaudo, C. (2017). Exit from Pluripotency Assay of Mouse Embryonic Stem Cells. Bio-Protocol *7*, e2507.

Cohen, D.M., and Chen, C.S. (2008). Mechanical control of stem cell differentiation.. https://www.stembook.org/node/516.

De Belly, H., Jones, P.H., Paluch, E.K., and Chalut, K.J. (2020). Membrane tension mediated mechanotransduction drives fate choice in embryonic stem cells. Cell Stem Cell *28*. Published online November 19, 2020. https://doi.org/10.1016/j.stem.2020.10.018.

Diz-Muñoz, A., Krieg, M., Bergert, M., Ibarlucea-Benitez, I., Muller, D.J., Paluch, E., and Heisenberg, C.-P. (2010). Control of directed cell migration in vivo by membrane-to-cortex attachment. PLoS Biol. *8*, e1000544.

Diz-Muñoz, A., Romanczuk, P., Yu, W., Bergert, M., Ivanovitch, K., Salbreux, G., Heisenberg, C.-P., and Paluch, E.K. (2016). Steering cell migration by alternating blebs and actin-rich protrusions. BMC Biol. *14*, 74.

Diz-Muñoz, A., Weiner, O.D., and Fletcher, D.A. (2018). In pursuit of the mechanics that shape cell surfaces. Nat. Phys. *14*, 648–652.

Engler, A.J., Sen, S., Sweeney, H.L., and Discher, D.E. (2006). Matrix elasticity directs stem cell lineage specification. Cell *126*, 677–689.

Farge, E. (2003). Mechanical induction of Twist in the Drosophila foregut/stomodeal primordium. Curr. Biol. *13*, 1365–1377.

Fehon, R.G., McClatchey, A.I., and Bretscher, A. (2010). Organizing the cell cortex: the role of ERM proteins. Nat. Rev. Mol. Cell Biol. *11*, 276–287.

Gauthier, N.C., Rossier, O.M., Mathur, A., Hone, J.C., and Sheetz, M.P. (2009). Plasma membrane area increases with spread area by exocytosis of a GPI-anchored protein compartment. Mol. Biol. Cell *20*, 3261–3272.

Gauthier, N.C., Fardin, M.-A., Roca-Cusachs, P., and Sheetz, M.P. (2011). Temporary increase in plasma membrane tension coordinates the activation of exocytosis and contraction during cell spreading. Proc. Natl. Acad. Sci. USA *108*, 14467–14472.

Gautreau, A., Louvard, D., and Arpin, M. (2000). Morphogenic effects of ezrin require a phosphorylation-induced transition from oligomers to monomers at the plasma membrane. J. Cell Biol. *150*, 193–203.

Guimarães, C.F., Gasperini, L., Marques, A.P., and Reis, R.L. (2020). The stiffness of living tissues and its implications for tissue engineering. Nat. Rev. Mater. *5*, 351–370.

Hackett, J.A., Dietmann, S., Murakami, K., Down, T.A., Leitch, H.G., and Surani, M.A. (2013). Synergistic mechanisms of DNA demethylation during transition to ground-state pluripotency. Stem Cell Reports *1*, 518–531.

Hackett, J.A., Huang, Y., Günesdogan, U., Gretarsson, K.A., Kobayashi, T., and Surani, M.A. (2018). Tracing the transitions from pluripotency to germ cell fate with CRISPR screening. Nat. Commun. *9*, 4292.

Hochmuth, F.M., Shao, J.Y., Dai, J., and Sheetz, M.P. (1996). Deformation and flow of membrane into tethers extracted from neuronal growth cones. Biophys. J. *70*, 358–369.

Houk, A.R., Jilkine, A., Mejean, C.O., Boltyanskiy, R., Dufresne, E.R., Angenent, S.B., Altschuler, S.J., Wu, L.F., and Weiner, O.D. (2012). Membrane tension maintains cell polarity by confining signals to the leading edge during neutrophil migration. Cell *148*, 175–188.

Hove, J.R., Köster, R.W., Forouhar, A.S., Acevedo-Bolton, G., Fraser, S.E., and Gharib, M. (2003). Intracardiac fluid forces are an essential epigenetic factor for embryonic cardiogenesis. Nature *421*, 172–177.

Kalkan, T., Olova, N., Roode, M., Mulas, C., Lee, H.J., Nett, I., Marks, H., Walker, R., Stunnenberg, H.G., Lilley, K.S., et al. (2017). Tracking the embryonic stem cell transition from ground state pluripotency. Development *144*, 1221–1234.

Karimi, M., Johansson, S., Stach, D., Corcoran, M., Grandér, D., Schalling, M., Bakalkin, G., Lyko, F., Larsson, C., and Ekström, T.J. (2006). LUMA (LUminometric Methylation Assay)–a high throughput method to the analysis of genomic DNA methylation. Exp. Cell Res. *312*, 1989–1995.

Korotkevich, E., Niwayama, R., Courtois, A., Friese, S., Berger, N., Buchholz, F., and Hiiragi, T. (2017). The Apical Domain Is Required and Sufficient for the First Lineage Segregation in the Mouse Embryo. Dev. Cell *40*, 235–247.e7.

Leeb, M., Dietmann, S., Paramor, M., Niwa, H., and Smith, A. (2014). Genetic exploration of the exit from self-renewal using haploid embryonic stem cells. Cell Stem Cell *14*, 385–393.

Leitch, H.G., McEwen, K.R., Turp, A., Encheva, V., Carroll, T., Grabole, N., Mansfield, W., Nashun, B., Knezovich, J.G., Smith, A., et al. (2013). Naive pluripotency is associated with global DNA hypomethylation. Nat. Struct. Mol. Biol. *20*, 311–316.

Li, J., Wang, Z., Chu, Q., Jiang, K., Li, J., and Tang, N. (2018). The Strength of Mechanical Forces Determines the Differentiation of Alveolar Epithelial Cells. Dev. Cell *44*, 297–312.e5.

Liu, Y., Belkina, N.V., Park, C., Nambiar, R., Loughhead, S.M., Patino-Lopez, G., Ben-Aissa, K., Hao, J.-J., Kruhlak, M.J., Qi, H., et al. (2012). Constitutively active ezrin increases membrane tension, slows migration, and impedes endothelial transmigration of lymphocytes in vivo in mice. Blood *119*, 445–453.

Louvet, S., Aghion, J., Santa-Maria, A., Mangeat, P., and Maro, B. (1996). Ezrin becomes restricted to outer cells following asymmetrical division in the preimplantation mouse embryo. Dev. Biol. *177*, 568–579.

Maître, J.-L., Turlier, H., Illukkumbura, R., Eismann, B., Niwayama, R., Nédélec, F., and Hiiragi, T. (2016). Asymmetric division of contractile domains couples cell positioning and fate specification. Nature *536*, 344–348.

Masters, T.A., Pontes, B., Viasnoff, V., Li, Y., and Gauthier, N.C. (2013). Plasma membrane tension orchestrates membrane trafficking, cytoskeletal

remodeling, and biochemical signaling during phagocytosis. Proc. Natl. Acad. Sci. USA *110*, 11875–11880.

Mulas, C., Kalkan, T., von Meyenn, F., Leitch, H.G., Nichols, J., and Smith, A. (2019). Defined conditions for propagation and manipulation of mouse embryonic stem cells. Development *146*, dev173146.

Murray, P., Prewitz, M., Hopp, I., Wells, N., Zhang, H., Cooper, A., Parry, K.L., Short, R., Antoine, D.J., and Edgar, D. (2013). The self-renewal of mouse embryonic stem cells is regulated by cell-substratum adhesion and cell spreading. Int. J. Biochem. Cell Biol. *45*, 2698–2705.

Niwa, H. (2007). How is pluripotency determined and maintained? Development *134*, 635–646.

North, T.E., Goessling, W., Peeters, M., Li, P., Ceol, C., Lord, A.M., Weber, G.J., Harris, J., Cutting, C.C., Huang, P., et al. (2009). Hematopoietic stem cell development is dependent on blood flow. Cell *137*, 736–748.

Pathak, M.M., Nourse, J.L., Tran, T., Hwe, J., Arulmoli, J., Le, D.T.T., Bernardis, E., Flanagan, L.A., and Tombola, F. (2014). Stretch-activated ion channel Piezo1 directs lineage choice in human neural stem cells. Proc. Natl. Acad. Sci. USA *111*, 16148–16153.

Przybyla, L., Lakins, J.N., and Weaver, V.M. (2016). Tissue Mechanics Orchestrate Wnt-Dependent Human Embryonic Stem Cell Differentiation. Cell Stem Cell *19*, 462–475.

Rauch, C., Brunet, A.-C., Deleule, J., and Farge, E. (2002). C2C12 myoblast/osteoblast transdifferentiation steps enhanced by epigenetic inhibition of BMP2 endocytosis. Am. J. Physiol. Cell Physiol. *283*, C235–C243.

Raucher, D., and Sheetz, M.P. (2000). Cell spreading and lamellipodial extension rate is regulated by membrane tension. J. Cell Biol. *148*, 127–136.

Stefani, C., Gonzalez-Rodriguez, D., Senju, Y., Doye, A., Efimova, N., Janel, S., Lipuma, J., Tsai, M.C., Hamaoui, D., Maddugoda, M.P., et al. (2017). Ezrin enhances line tension along transcellular tunnel edges via NMIIa driven actomyosin cable formation. Nat. Commun. *8*, 15839.

Toyooka, Y., Shimosato, D., Murakami, K., Takahashi, K., and Niwa, H. (2008). Identification and characterization of subpopulations in undifferentiated ES cell culture. Development *135*, 909–918.

Trappmann, B., Gautrot, J.E., Connelly, J.T., Strange, D.G.T., Li, Y., Oyen, M.L., Cohen Stuart, M.A., Boehm, H., Li, B., Vogel, V., et al. (2012). Extracellular-matrix tethering regulates stem-cell fate. Nat. Mater. *11*, 642–649.

Welf, E.S., Miles, C.E., Huh, J., Driscoll, M.K., Isogai, T., Noh, J., Weems, A.D., Chi, J., Pohlkamp, T., Dean, K., et al. (2019). A unified role for membrane-cortex detachment during cell protrusion initiation. bioRxiv. https://doi.org/10.1101/696211.

Wray, J., Kalkan, T., Gomez-Lopez, S., Eckardt, D., Cook, A., Kemler, R., and Smith, A. (2011). Inhibition of glycogen synthase kinase-3 alleviates Tcf3 repression of the pluripotency network and increases embryonic stem cell resistance to differentiation. Nat. Cell Biol. *13*, 838–845.

STAR★METHODS

KEY RESOURCES TABLE

REAGENT or RESOURCE	SOURCE	IDENTIFIER
Antibodies		
Nanog Monoclonal Antibody (eBioMLC-51), eBioscience	Thermo Fisher Scientific	Cat# 14-5761-80; RRID: AB_763613
Goat anti-Rat IgG (H+L) Cross-Adsorbed Secondary Antibody, Alexa Fluor 647	Thermo Fisher Scientific	Cat# A-21247
Chemicals, Peptides, and Recombinant Proteins		
PD0325901	Tocris	Cat# 4192
CHIR99021	Tocris	Cat# 4423
LIF (Leukemia inhibitory factor)	EMBL Protein Expression and Purification Core Facility	N/A
EmbryoMax ES Cell Qualified FBS	Merck	Cat# ES-009-C
FGF2	PeproTech	Cat# 450-33
Activin A	PeproTech	Cat# 120-14E
Critical Commercial Assays		
JPK CellHesion200 (AFM)	Bruker	https://www.bruker.com/products/surface-and-dimensional-analysis/atomic-force-microscopes.html
OBL-10 cantilever	Bruker	Cat# OBL-10
Deposited Data		
RNA-seq	this study	ArrayExpress: E-MTAB-9404 (https://www.ebi.ac.uk/arrayexpress/experiments/E-MTAB-9404/)
Experimental Models: Cell Lines		
mESC Rex1-GFPd2	Austin Smith's laboratory (Cambridge Stem Cell Institute)	N/A
Recombinant DNA		
Plasmid: pPB-TRE_CAEzrin_CAG-Tet3G-IN	this study	N/A
Plasmid: pPB-TRE_DNEzrin_CAG-Tet3G-IN	this study	N/A
Plasmid: pPB-TRE_iMC-linker_CAG-Tet3G-IN	this study	N/A
Plasmid: pPB-TRE_mCherry_CAG-Tet3G-IN	this study	N/A
Plasmid: pPB-TRE_PMBD_CAG-Tet3G-IN	this study	N/A
Plasmid: pPB-TRE_ABD_CAG-Tet3G-IN	this study	N/A
Software and Algorithms		
FlowJo	BD (Becton, Dickinson & Company)	https://www.flowjo.com/
R	The R Project	https://www.r-project.org/
JPK SPM Destkop	Bruker	https://www.bruker.com/products/surface-and-dimensional-analysis/atomic-force-microscopes.html
JPK Data Processing	Bruker	https://www.bruker.com/products/surface-and-dimensional-analysis/atomic-force-microscopes.html

RESOURCE AVAILABILITY

Lead contact

Further information and requests for resources and reagents should be directed to and will be fulfilled by the Lead Contact, Alba Diz-Muñoz (diz@embl.de).

Materials availability

Plasmids and stable mES cell lines generated during this study are available from the lead contact on request.

Data and code availability

The accession number for the RNA-sequencing datasets reported in this paper is ArrayExpress: E-MTAB-9404 (https://www.ebi.ac.uk/arrayexpress/experiments/E-MTAB-9404/).

EXPERIMENTAL MODEL AND SUBJECT DETAILS

Cell culture

Male mESCs expressing Rex1-GFPd2 (Toyooka et al., 2008; Wray et al., 2011) were kindly provided by the Austin Smith's laboratory (Cambridge Stem Cell Institute). These cells express a GFP reporter from the promoter of Rex1, a canonical naive pluripotency marker. Cells have been authenticated as mESC based on their successful contribution to chimeras (Leeb et al., 2014). Naive cells were maintained in DMEM medium containing 15% EmbryoMax ES Cell Qualified FBS (Merck) and LIF (10 μg/ml, EMBL Protein Expression Facility) or in serum-free N2B27 medium containing 2i (1 μM PD0325901and 3 μM CHIR99021, both Tocris) and LIF (10 μg/ml) on polystyrene culture dishes coated with 0.1% (w/v) Gelatin (Sigma) solution at 37°C with 5% CO_2. Primed cells were cultured similarly in N2B27 medium containing 12 ng/ml FGF2 and 20 ng/ml Activin A (both PeproTech). N2B27 medium was prepared from a 1:1 mixture of DMEM/F12 (without HEPES, with L-glutamine) and neurobasal medium (no L-glutamine), supplemented with 0.5 × B-27 (without vitamin A) and 0.5 × N-2 supplement, 100 U/ml penicillin and 100 μg/ml streptomycin, 2.5 mM L-glutamine (all Thermofisher), 10 μg/ml BSA fraction V and 10 μg/ml human recombinant insulin (both Sigma). Medium was changed every other day and cells were passaged using 0.05% Trypsin-EDTA (Thermofisher) at ratios of 1/4–1/10.

To induce differentiation and exit from naive pluripotency, mESCs originating from 2i/LIF culture were plated on Gelatin-coated culture-dishes at a density of about 40.000/square cm in plain N2B27 medium (or 2i/LIF medium as control) and cultured for 48 h. Expression of constructs was induced by adding 1 μg/ml doxycycline (Dox; Sigma) at the time of seeding.

To induce formation of embryoid bodies (EBs) mESCs originating from Serum+LIF culture were seeded on non-coated (i.e., non-adhesive) culture-dishes at a density of about 80.000/square cm in medium without LIF to allow for spontaneous differentiation. Expression of constructs was induced by adding 1 μg/ml doxycycline (Dox) at the time of seeding. EBs were grown for 96 h. Medium was exchanged after 48 h.

Stable cell line generation

To generate stable cell lines with inducible constructs, sequences of interest were cloned into a PiggyBac vector expressing a Neomycin resistance gene (pPB-TRE_CAG-Tet3G-IN). Stable integration was achieved by co-transfecting the PiggyBac plasmid and a plasmid encoding the PiggyBac transposase using Lipofectamine 3000 (Thermofisher), followed by selection with 400 μg/ml Geneticin (Thermofisher). Single colony clones were finally screened for low background expression levels and matching expression levels upon induction.

Inducible (*ind*-) cell line	Construct name	Construct description	Residues or mutations
mESC Rex1-GFPd2 *ind*-CAEz	CAEzrin	constitutively active version of human Ezrin, fused to mCherry	T567D
mESC Rex1-GFPd2 *ind*-DNEz	DNEzrin	dominant negative version of human Ezrin, fused to mCherry	T567A
mESC Rex1-GFPd2 *ind*-mCherry	mCherry	mCherry	//
mESC Rex1-GFPd2 *ind*-PMBD	plasma membrane-binding domain (PMBD)	human Tyrosine-protein kinase lyn lipidation motif, fused to mCherry	Residues 1-13 (Gauthier et al., 2011)
mESC Rex1-GFPd2 *ind*-ABD	actin-binding domain (ABD)	mCherry fused to Human utrophin actin binding domain (CH-CH)	Residues 1-246 (Houk et al., 2012; Raucher and Sheetz, 2000)
mESC Rex1-GFPd2 *ind*-iMC	iMC-linker	PMBD-mCherry-ABD	//

METHOD DETAILS

Re-plating assay

Cells were allowed to exit from naive pluripotency in plain N2B27 medium. After 48 h, cells were resuspended and counted using trypan blue. A specific number of living cells (typical density: 5000-10.000/cm^2) was then re-plated in 2i/LIF medium. After 4-6 days, the number of colonies was manually counted. This assay quantifies the efficiency of pluripotency exit, as only naive cells survive in 2i/LIF medium (Mulas et al., 2019).

Flow cytometry

Cells were dissociated to single-cell suspension with 0.05% Trypsin-EDTA (Thermofisher), resuspended in PBS supplemented with 0.1% BSA and 2.5 mM EDTA, strained through a 40 μm cell strainer (BD Biosciences) and analyzed on an LSRFortessa flow cytometer (BD BioSciences). Flow cytometry data were gated on forward and side scatters using the FlowJo software. Occasionally, DAPI was added as live-dead-stain to the cells and data were gated further on DAPI fluorescence to check for cellular integrity. Fluorescent levels of individual populations were quantified by their geometric means.

Tether extrusion by atomic force spectroscopy

Apparent membrane tension and MCA were measured extruding plasma membrane tethers. In brief, OBL-10 cantilevers (Bruker) were mounted on a CellHesion 200 AFM (Bruker) which is integrated into an Eclipse Ti inverted light microscope (Nikon). Cantilevers were then calibrated using the thermal noise method (spring constant ~60 pN/nm) (reviewed in Gauthier et al., 2011; Houk et al., 2012) and coated with 2.5 mg/ml Concanavalin A (Sigma) for 1 h at 37°C. Before the measurements, cantilevers were rinsed in PBS. For the measurements, cells were seeded on Cellview glass bottom dishes (Greiner) or 35 mm low μ-Dishes (Ibidi) filled with N2B27 medium with or without 2i/LIF according to the experiment.

Measurements were run as follows: approach velocity was set to 0.5 μm/s while contact force and contact time were varied between 100 to 200 pN and 100 ms to 10 s respectively, aiming at maximizing the probability to extrude single tethers. Apparent membrane tension was measured using the static tether method: to ensure tether breakage at 0 velocity, the cantilever was retracted for 10 μm at a velocity of 10 μm/s. The position was then kept constant for 20 s and tether force at the moment of tether breakage was recorded at a sampling rate of 2000 Hz. MCA was measured using the dynamic tether method: each cell was probed multiple times at different pulling velocities (2, 5, 10, 30 μm/s) in a random order; only tethers which broke during the pulling phase were considered. Tethers were allowed to retract completely between successive pulls. Resulting force–time curves were analyzed using the JPK Data Processing Software. Measurements were run at 37°C with 5% CO_2 and samples were used no longer than 1 h for data acquisition.

Tether data analysis and model assumptions

Static tether puling: apparent plasma membrane tension (the sum of in-plane tension (T_m) and MCA (γ)) depends on the breakage tether force (f_0) and the bending rigidity of the membrane (κ). We used a previously measured value for κ ($2.7*10^{-19}$ Nm; Brochard-Wyart et al., 2006; Hochmuth et al., 1996), which we assumed was unchanged upon exit from naive pluripotency:

$$T = T_m + \gamma = \frac{f_0^2}{8\pi^2\kappa}$$

Dynamic tether pulling: To estimate the contribution of MCA, plasma membrane tethers were pulled at different retraction velocities (v), where the tether force (f) increases with increasing velocity. To interpret such measurements, the Brochard-Wyart et al. model was applied to the data using Monte-Carlo based fitting (Brochard-Wyart et al., 2006):

$$f^3 - ff_0^2 = av = \left[(2\pi)^3 2\kappa^2\eta\varepsilon \ln\left(\frac{R_c}{R_t}\right)\right]v$$

Since the radius of the cell (R_c) >> radius of the tether (R_t), and bending rigidity κ is assumed to be constant, the tether force increase with pulling velocity depends only on surface viscosity (η) and the density of the MCA linkers (ε). The term $\eta\varepsilon$ thus reflects the effect of MCA: the larger the extent of MCA, the higher is the drag of the lipids around integral membrane proteins connected to the underlying cortex. In this work, we report the parameter *a* as a proxy for MCA, as $\eta\varepsilon$ is proportional to *a* and we assume R_c, R_t and κ to be constant.

Scanning electron microscopy

For scanning electron microscopy imaging, Rex1-GFPd2 mESCs were cultured for 24 h on glass coverslips previously cleaned, plasma treated for 2 min and coated with 0.1% Gelatin (Sigma), 10 μg/ml human fibronectin (Corning) or 5 μg/ml Laminin 511 (Biolamina). Cells were fixed for 30 min at room temperature with 4% (w/v) formaldehyde (EMS) and 2.5% (w/v) glutaraldehyde (EMS) dissolved in 0.1 M PHEM buffer (60 mM PIPES; 25 mM HEPES; 10 mM EGTA; 2 mM Magnesium chloride; pH 6.9). Afterward, rinsing in PHEM buffer and water, post-fixation with 1% (w/v) osmium tetroxide (EMS) in water and 0.8% potassium hexacyanoferrate (III) (EMS) in water, 1% (w/v) tannic acid (EMS) in water and 1% (w/v) uranyl acetate (Serva) in water, and dehydration in ascending series of ethanol and drying in ascending series of HMDS (Sigma-Aldrich) were performed using microwave-assisted processing (Biowave Pro, Pelco). Prior to imaging, a layer of gold was sputter-coated onto the sample (Quorum Q150RS). Cells were acquired with either the Teneo (Thermofisher) or the Crossbeam-540 (Zeiss) at an accelerating voltage of 5 kV detecting secondary electrons. Cell area was quantified manually using Fiji.

RNA-sequencing

10^5 to 10^7 cells were pelleted via centrifugation and total RNA was extracted with the mirVana miRNA Isolation Kit (Thermofisher) according to the manufacturers recommendations. NGS Libraries were prepared and sequenced by the EMBL Genomics Core Facility. The obtained mRNA sequencing reads were mapped against the mouse genome (GRCm38) using STAR (with default options). Read per gene counts were produced during alignment (–quantMode) based on GRCm38.83 annotation. The obtained

raw read counts were processed as follows: Genes with less than 1 count-per-million reads (cpm) in half the samples were removed using the *cpm* function in the edgeR library. Next, the *voom* function in the *limma* package was used to normalize the read counts and a linear model to the normalized data were applied for identification of differentially expressed genes. Genes with false discovery rate (FDR) corrected p value < 0.05 and fold change of > 1 were considered as differentially expressed genes. ggplot2 in R was used for data visualization. Pathway map enrichments were performed using the *enrichR* package and the KEGG (Kyoto Encyclopedia of Genes and Genomes) database.

Nanog immunofluorescence

Cells were fixed in suspension in 4% formaldehyde in PBS for 20 min on ice. Next, cells were permeabilized and blocked in 1% FBS, 1% BSA and 0.1% Triton-X in PBS for 1 h on ice. The primary antibody (Nanog Monoclonal Antibody eBioMLC-51, Thermofisher) was diluted 1:200 in the same blocking buffer and cells were incubated at 4°C overnight, followed by a single washing step in blocking buffer for 10 min at room temperature. The secondary antibody (Goat-anti-Rat Alexa Fluor 647, Thermofisher) was diluted 1:600 in the blocking buffer and cells were incubated for 1 h at room temperature. After a final washing step in blocking buffer for 10 min, fluorescence levels were analyzed quantitatively using flow cytometry.

DNA methylation analysis

LUMA was used to measure the global CpG methylation status (Karimi et al., 2006). In brief, genomic DNA from mESCs was isolated using the Quick-DNA Microprep Plus Kit (Zymo Research, #D4074) and quantified using Qubit III. Each sample of genomic DNA (75-150ng) was digested in two parallel reactions at 37°C for 4 h with HpaII or MspI and EcoRI as an internal control for both reactions. Overhangs from both reactions were then analyzed using the PyroMark Q24 Advanced system from QIAGEN, with the dispensation order GTGTGTCACACAGTGT. Percentage of genome-scale methylated CpGs was determined by comparing the EcoRI normalized HpaII signal intensity ratio to the normalized MspI signal intensity ratio using the following equations:

$$HpaII\ ratio : \frac{Dispensation\ 7+13}{\left(\frac{Dispensation\ 8+14}{2}\right)}$$

$$MspI\ ratio : \frac{Dispensation\ 7+13}{\left(\frac{Dispensation\ 8+14}{2}\right)}$$

$$\%\ mCpG\ : 100\% \times \left(1 - \frac{HpaII\ ratio}{MspI\ ratio}\right)$$

QUANTIFICATION AND STATISTICAL ANALYSIS

Data were analyzed, tested for statistical significance, fitted, and visualized using R. No statistical method was used to predetermine sample size. No estimation of variance was performed. The Shapiro–Wilk test was used to test for normality of data. Welch's t test was chosen for statistical testing of normal distributed data with low sample size (n < 30). For non-normal distributed data with low sample size (n < 30), Mann-Whitney U-test was performed. For large sample sizes (n > 30), the *Z*-Test was used. n.s. depicts non-significant changes.